Integrated approach for data acquisition, visualization and processing of analog polarographic systems for bioenergetics studies

Potter L[1,2], Krusienski D[3], Kennedy J[1], Hoppel CL[5,6,7], Lai N[1,2,4,8*]

[1]*Department of Electrical and Computer Engineering;* [2]*Biomedical Engineering Institute; Old Dominion University, Norfolk, Virginia,* [3]*Department of Biomedical Engineering Virginia Commonwealth University, Richmond, Virginia,* [4]*Department of Biomedical Engineering,* [5]*Center for Mitochondrial Disease;* [6]*Department of Pharmacology and,* [7]*Department of Medicine, School of Medicine, Case Western Reserve University;* [8]*Department of Mechanical, Chemical and Materials Engineering, University of Cagliari*

*Corresponding author
Nicola Lai, PhD
Associate Professor
Department of Electrical & Computer Engineering
Biomedical Engineering Institute
231 Kaufman Hall
Old Dominion University
Norfolk, VA 23529
Phone: 757-683-6062
Email: nlai@odu.edu

Keywords: Mitochondria, Kinetics, Computational methods, Software, Respiration rate, ADP/O ratio

Abstract

Bioenergetic function is characterized with assays obtained by polarographic systems. Analog systems without data acquisition, visualization, and processing tools are used but require cumbersome operations to derive respiration rate and ADP to oxygen stoichiometry of oxidative phosphorylation (ADP/O ratio). The analog signal of a polarograhic system (YSI-5300) was digitized and a graphical user interface (GUI) was developed in MATLAB to integrate visualization, recording, calibration and processing of bioenergetic data. With the GUI, the signal is continuously visualized during the experiment and respiratory rates and ADP/O ratios can be determined. The integrated system was tested to evaluate bioenergetic function of subpopulations of mitochondria isolated from rat skeletal muscle (n=10). Signal processing was applied to denoise data recorded at the sampling rate of 1000Hz, and maximize data decimation for computational applications. The error in calculating the bioenergetic outputs using decimated data is negligible when data are denoised. The estimate of respiration rate, ADP/O ratio and RCR obtained with denoised data at sampling rate as low as 5Hz was similar to that obtained with raw data recorded at sampling rate of 1000Hz.

In summary, the integrated tools of the GUI overcome the limitations of data processing, accuracy, and utilization of analog polarographic systems.

1.Introduction

Polarographic methods have been essential to measure the concentration and flux of oxygen in biological samples. After early studies on mitochondrial bioenergetics [1], major limitations of the polarographic methods were overcame with the Clark electrode [2, 3] one of the first membrane-covered amperometric oxygen electrode with enhanced lifetime and stability. The design of this oxygen sensor evolved for decades to provide advanced oxygen detection for medical and research applications [4, 5]. The polarographic system based on the Clark electrode is commonly used for bioenergetics studies in mammals [6] and plants [7, 8] to measure cellular respiration and photosynthesis, respectively.

To evaluate cellular bioenergetics, mitochondrial respiratory rate is typically measured under different experimental conditions such as state 3 and 4. Therefore, oxidative phosphorylation rate, respiratory control ratio (RCR) and ADP/O ratio are outcomes derived by the analysis of the mitochondrial oxygen kinetics measured with different experimental apparatus. There are polarographic (Hansatech Instruments Ltd, Oroboros Instruments, Strathkelvin Instruments, Yellow Springs Instrument, YSI) and fluorescence systems (Seahorse XF Analyzers) with an integrated data acquisition, visualization and processing tools [8-13] to analyze bioenergetics data. Some of the polarographic systems without these integrated features are still popular, valuable, and viable tools [14-33]. In some cases, a flatbed recorder is used [24, 26, 27], in other cases, data are digitized [14, 28-33] and analyzed with commercial software [25]. Also, data acquisition devices allow digitization at high sampling rate (e.g. 1000Hz), but in some cases generate an excess of recorded data leading to an increase processing time and unnecessarily large files. The sampling rate should be optimized considering the signal changes with time in studying mitochondrial kinetics and signal to noise ratio. Thus, an approach integrating data acquisition, visualization, denoise is desirable to analyze data of these existing systems.

A GUI (graphical user interface) was developed in MATLAB to integrate digitization, visualization, and processing of bioenergetics data measured with a biological oxygen monitor YSI 5300 with a Clark electrode. The integrated system can be used to calibrate, record, and continuously visualize the signal during the experiment, as well as determine respiratory rates and ADP/O ratio. A signal processing approach is applied to reduce the noise and decimate for computational applications.

2.Methods

2.1.Polarographic System

The system was designed by mitochondrial physiologists for bioenergetics experiments. The polarographic system was composed of a 2-Channel biological oxygen monitor (YSI 5300, Yellow Springs Instrument, Ohio), oxygen electrode (YSI 5331, 34) , custom made metabolic chamber with a water jacket connected to a heated water circulator (Polyscience, MX15H135-A11) to control the temperature (Fig. 1). The solution of the metabolic chamber was mixed with a magnetic stirrer (VWR Dylastir). To digitize the analog signal from the biological oxygen monitor the NI-DAQ (National Instruments-Data Acquisition Device) USB-6001 was used to connect the electrode to a personal computer. A graphical user interface was developed in MATLAB to perform acquisition, denoising, and storage of the digitized data.

Figure 1

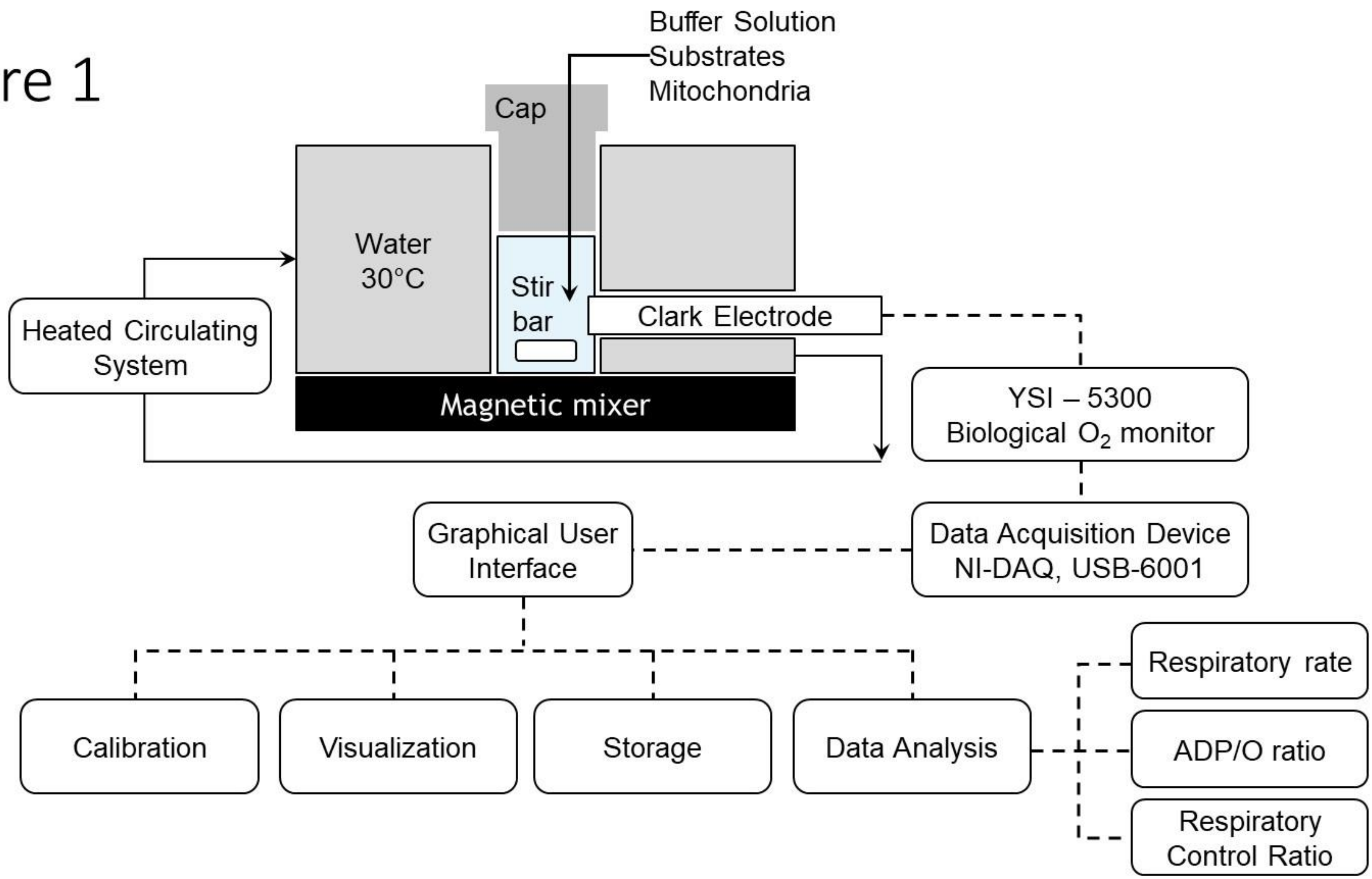

Figure 1. Schematic representation of the polarographic system with the data acquisition device and graphical use interface.

2.2. Experimental Protocol

The experimental protocol conformed to the guide for the care and use of laboratory animals published by the National Research Council [35] and was approved by the Old Dominion Institutional Animal Care and Use Committee. Ten male Wistar rats (Charles River Laboratories, MA) were housed and fed a standard diet chow in the animal facilities of Old Dominion University with 12:12-h light-dark cycle.

Subsarcolemmal (SSM) and interfibrillar (IFM) mitochondria were isolated from rat vastus lateralis using the protocol developed by our group [36]. The Lowry method was used to determine mitochondrial protein concentration [37]. Oxygen consumption by SSM and IFM was determined with a GUI connected to the polarographic system with a final volume of 0.5 mL respiration buffer at 30ºC. An ADP concentration of 0.1 mM was used to deplete endogenous substrates before glutamate (20 mM) was added and the mitochondria stimulated with 0.2 mM ADP (ADP-stimulated) to measure State 3 respiration rate. After ADP depletion, State 4 respiration was measured (ADP-limited). The concentration of glutamate, uncoupler, and ADP refers to the initial concentrations in the chamber. State 3 and 4 respiration rates were measured twice. Then to determine maximal oxidative phosphorylation, the respiratory rate was measured in the presence of a saturated concentration of ADP, 2 mM. Finally, 0.2 mM of the uncoupler dinitrophenol (DNP) was added to the chamber to measure oxidative capacity of the electron transport chain. Respiratory control ratio (RCR, State 3 divided by State 4) quantifies the control of oxygen consumption by adenosine nucleotide translocator, phosphate transporter, and phosphorylation (‘coupling’). The concentration of the ADP and AMP were determined with an enzymatic method [38] and used to calculate the ADP/O ratio (ADP mole added per mole of oxygen atom consumed).

2.3.Graphical User Interface

A graphical user interface was developed in MATLAB [39] to integrate four modules: acquisition and storage, visualization, calibration, and analysis of the data. These modules allow the user to perform the following tasks: a) acquire and record the data in an excel file; b) calibrate the electrode and store calibration parameters; c) visualize the oxygen concentration within the metabolic chamber during the experiment; d) perform analysis of the data after the experiment is completed to determine respiratory rates, RCR, and ADP/O ratios. Also, the GUI can visualize and analyze data in comma separated values format obtained with other digitized systems.

The NI-DAQ was a 14-bit analog-to-digital converter used with a sampling rate of 1000 Hz. The MATLAB data acquisition toolbox was used to handle the communication of the data from the oxygen monitor to the computer. The data were filtered with the MATLAB library "*mean*" [39] for continuous visualization of the data during the experiment. A user guide of the GUI and video tutorials to show how to use the GUI are available at the data repository folder. (https://data.mendeley.com/datasets/zb3d696s5c/draft?a=66238101-acbe-4d5b-afdd-b38342ebaef1)

2.4.Calibration

The polarographic electrode signal ranged between 0 and 1 volt. The oxygen-dependent voltage signal from the biological oxygen monitor was converted to oxygen concentration with a calibration obtained with a physiological buffer for bioenergetics experiments [40]. The molecular oxygen concentration in the medium was previously determined to be 222.5 nmol mL^{-1} at 30°C and atmospheric pressure [38, 41, 42]. This value of oxygen solubility was reported in the option pane of the software and used by the software to relate the voltage measurement to the oxygen concentration within the chamber at a specific temperature. The electrode of the polarographic oxygen sensor was calibrated with a measurement of the voltage signal obtained with two distinct oxygen contents dissolved in a mixed buffer media of 0.5 mL within the bioreactor at 30°C under the following experimental conditions: a) a gas-liquid equilibrium between room air and media; and b) in presence of sodium dithionite to consume the oxygen dissolved in the media. The oxygen dissolved in the buffer under thermodynamic equilibrium was previously established and used as input for the conversion factor. The parameter of the calibration was determined and stored in a comma-separated values format for the experiment.

2.5.Data analysis

The data analysis module of the GUI was utilized to calculate the state 4 respiratory rate, state 3 respiratory rate with an unsaturated or saturated ADP concentration, and uncoupled respiratory rate by linear regression (‘*regress*’, MATLAB library) [39] of the raw data (i.e. 1000Hz), which was selected graphically using the mouse by the user. The respiratory rate was normalized to the amount of the biological sample (e.g. mg of mitochondrial proteins) and expressed as pmol of O_2 $s^{-1}mg^{-1}$. Also, the software was used to compute the amount of oxygen utilized during phosphorylation of the injected amount of ADP [43]. These data were used to calculate ADP/O ratio.

To reduce the sampling rate of the data recorded without significantly affecting the respiration rates, RCR, and ADP/O ratio values obtained with the raw data recorded at 1000 Hz, the data were denoised in four steps and decimated in the last step of the denoising process. The four steps included: 1) the time profile of the oxygen concentration was converted with Fast Fourier Transform (FFT) to the frequency domain and the isolated spurious spectral peaks were removed by setting them to zero; 2) data were converted from the frequency to the time domain with the inverse Fast Fourier Transform (iFFT); 3) data were processed to remove linear trends using the MATLAB library "*detrend*" [39] with a window of 0.1 seconds; 4) data were filtered to remove signals with high frequency and decimated to different sampling rates (5, 10, 20, 50, 100, and 500 Hz) using the Matlab library ("*decimate*") [39]. This function allows to filter and down sampling the data at once. A Chebyshev type I infinite impulse response (IIR) filter of order 8 was used with a corner frequency based on the desired sampling rate.

To analyze the effects of the sampling rate on the biochemical outputs of the data analysis, the respiratory rates, RCR, and ADP/O ratio were calculated for both raw and denoised and decimated data at different sampling rate (f) 5, 10, 20, 50, 100, and 500 Hz using the same interval of time for regression of the data recorded at 1000 Hz. At each sampling rate, the mean percentage error (e_f) in determining state 4, state 3 (with unsaturated or saturated ADP concentration), and uncoupled respiratory rates as well as RCR and ADP/O ratio relative to that obtained with a sampling rate of 1000 Hz was calculated for raw and denoised data as follows:

$$e_f = 100 \sum_{i=1}^{m} \left| X_{1000Hz} - X_f \right| / X_{1000Hz} \qquad (1)$$

where X_{1000Hz} and X_f represent the value obtained with a sampling rate of 1000 Hz and f, respectively, and m was the number of data available. For both SSM (n=10) and IFM (n=10), the relative error was estimated for each respiration rate (State 3, State 4, uncoupled), RCR, and ADP/O ratios.

2.6.Statistical Analysis

Results are reported as means ± standard deviation. Differences between SSM and IFM data were analyzed by a student's paired t test with two tails. The comparisons of the relative error obtained at different sampling rate between raw and denoised data were evaluated with two-way

ANOVA and Bonferroni correction for multiple comparisons. This analysis was performed for both SSM and IFM. Difference of $p<0.05$ was considered significant.

3.Results

3.1.Graphical user interface

The graphical user interface (GUI) is developed to have a window with a control panel to run calibration and experiment as well as define the experimental settings (sampling rate, calibration setting, biological sample amount, ADP injected). A representative time profile of the mitochondrial oxygen kinetics recorded with the GUI is reported in Fig. 2. The unfiltered and filtered data (1000 Hz) were reported in gray and black lines, respectively. The data are stored in a comma separated values file format and can be analyzed with the GUI tools. Once the collected data are visualized with the GUI, the data tools embedded in MATLAB are used with the mouse to select the interval of data for linear regression necessary to estimate the oxygen consumption rate. Two short vertical lines are visualized to delimitate the interval of the data selected. The button "JO2" allows the user to perform the regression to calculate the fluxes J_1, J_2, J_3, J_4, J_5, J_6, and J_7 (Fig. 2). Thus, GUI is used to determine specifically, state 3 with unsaturated ADP (J_2, J_4), or saturated ADP (J_6) concentration, state 4 (J_3, J_5), and uncoupled (J_7) respiratory rates, as well as, RCR. The software uses the intersection of the regression lines corresponding to the flux J_1 and J_2 and that of the lines of the flux J_2 and J_3 to determine the oxygen utilized to phosphorylate the amount of ADP (0.2 mM) injected to the chamber. Thus, the oxygen utilized is visualized by the vertical dotted black line which represents the vertical distance between the two intersections. The button "ADP/O" allows the user to calculate the ratio between the oxygen consumed and the amount of ADP injected. Similarly, the regression lines corresponding to the fluxes J_3, J_4 and J_5 are used to determine the ADP/O ratio for the second injection of ADP at 0.2 mM.

The respiration rates normalized to the amount of biological sample, as well as the RCR and ADP/O ratios are stored in a cvs format file for future analysis.

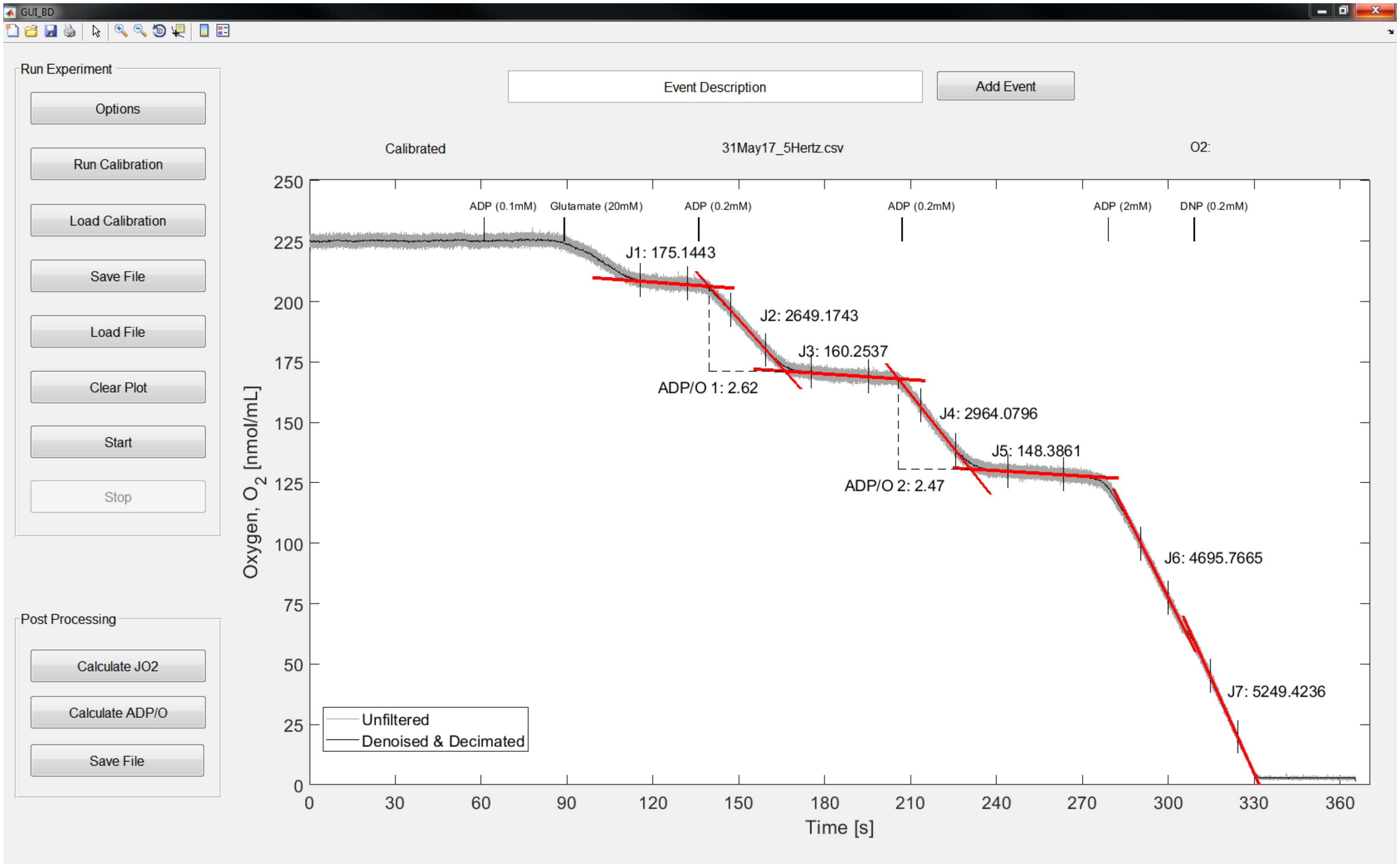

Figure 2. A representative time profile of the oxygen kinetics during a mitochondrial respiration stimulation: filtered data (black) and unfiltered data (grey) with the results of the data analysis tools of the GUI to estimate the respiration rates and ADP/O ratios.

3.2.Mitochondrial yield and oxidative phosphorylation

The SSM yield is 36% that of the IFM yield (Table 1). In the presence of glutamate, state 3 respiratory rate of SSM with an unsaturated ADP concentration is similar to that observed for IFM. The respiration rate with a saturated concentration of ADP significantly increases (15%) for both SSM and IFM. The maximal State 3 respiratory rate of SSM is significantly lower than that measured for IFM. Oxidative phosphorylation and uncoupling respiratory rates of IFM are approximately 10% higher than those observed for SSM. The RCR values for SSM and IFM are 18 (Table 1) and ADP/O ratios for SSM and IFM are approximatively equal to 2.77.

	Unit	**SSM**	**IFM**	***p***
Yield	[mg g^{-1}]	2.16±0.6	6.5±0.7*	10^{-10}
State 3	[pmol $s^{-1}mg^{-1}$]	2680±372	2776±263	10^{-1}
State 4	[pmol $s^{-1}mg^{-1}$]	194±44	144±19*	10^{-2}
RCR	[-]	15.1±6	20±3*	3 10^{-2}
ADP/O	[-]	2.77±0.26	2.80±0.21	7 10^{-1}
High ADP	[pmol $s^{-1}mg^{-1}$]	3913±536	4297±509*	10^{-4}
Uncoupled	[pmol $s^{-1}mg^{-1}$]	4482±623$^{¥}$	4890±586$^{¥,*}$	10^{-3}

Table 1. Mitochondrial yield and oxidative phosphorylation characteristics of skeletal muscle subsarcolemmal mitochondria (SSM) and interfibrillar mitochondria (IFM) from vastus lateralis. The respiratory rate is related to mg of mitochondrial protein. Values are obtained with raw data and reported as means ± standard deviation (n=10).

RCR: respiratory control ratio;
ADP/O: ADP to oxygen ratio;
High ADP: Saturated concentration of ADP;
DNP: Uncoupling state in presence of dinitrophenol;
* Significantly different from SSM.
$^{¥}$ Significantly different from high ADP.

3.3.Denoised effects on sampling rate

To analyze the noise of the data, the unfiltered data was subtracted from the denoised data for each time point and reported in Fig. 3a. The distribution of this difference follows a Gaussian distribution as reported in Fig. 3b.

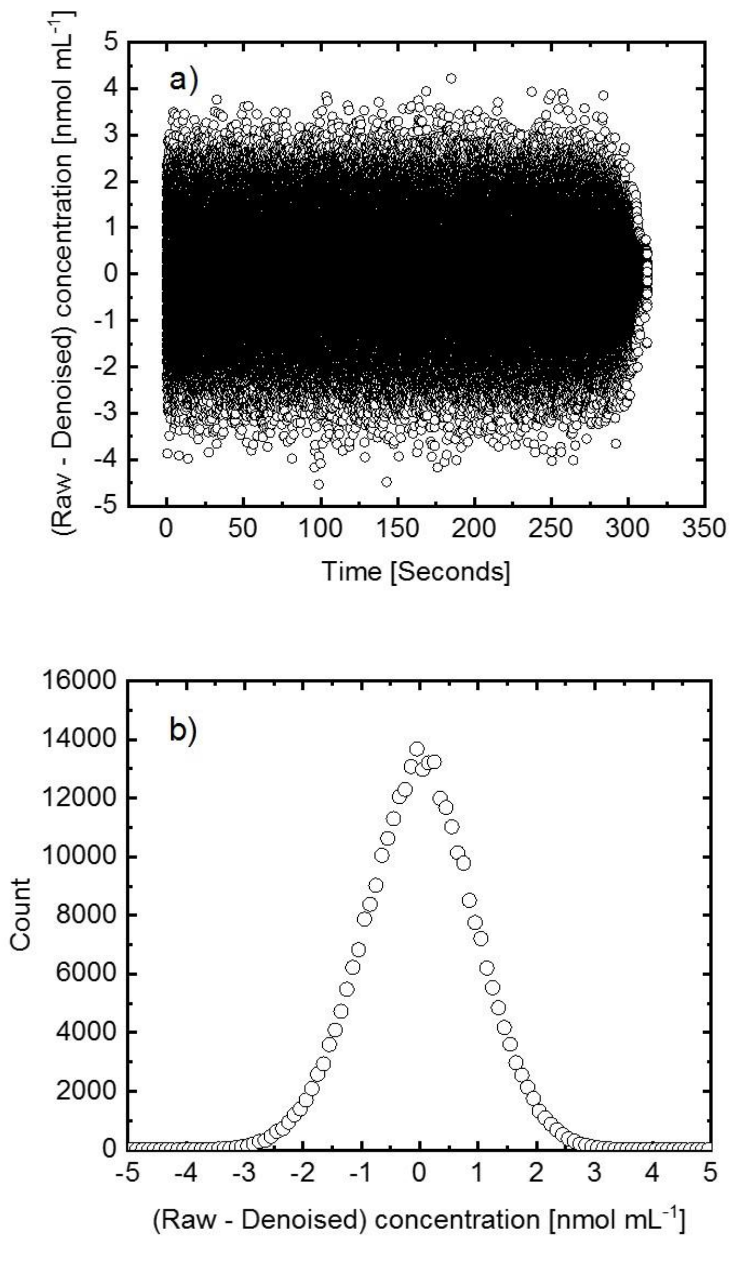

Figure 3. The difference between the raw and denoised concentration data (a) at each time point and its statistical distribution (b).

The respiratory state 3, state 4, and uncoupled rates as well as ADP/O and RCR obtained with a sampling rate of 1000 Hz (Table 1), were re-estimated using the raw and denoised data collected at sampling rates of 500, 100, 50, 20, 10, and 5 Hz (Fig. 4, 5 and 6) for both SSM and IFM.

In SSM, the relative error of the respiration rates obtained with raw data (Fig.4 and 5) increase with a decrease of the sampling rate from 1000 to 5 Hz. This error became significantly different from zero for respiratory rate with: unsaturated ADP concentration at sampling rate lower than 100 Hz ($p<10^{-3}$, Fig. 4a); saturated ADP concentration at sampling rate lower than 10 Hz ($p<10^{-15}$, Fig. 4b), uncoupled mitochondria at sampling rate lower than 20 Hz ($p<10^{-3}$, Fig. 4c). In addition, when the relative error of the respiration rates obtained with raw data was significant at a specific sampling rates, it was greater than that with denoised data for the same sampling rate. Furthermore, the relative error for all respiratory rates obtained with denoised data was not significantly different from zero regardless the sampling rate.

In SSM, the relative error in calculating state 4 respiratory rate (Fig. 5) increases with a decrease of the sampling rate for both raw and denoised data. For a decrease of the sampling rate from 500 to 5 Hz, the relative error of state 4 respiratory rate obtained with raw data increased from 1±1 to 19±14%. Also, the relative error for ADP/O ratio (Fig. 6a) and RCR (Fig. 6b) obtained with raw data increased from 0.07±0.04 to 1.2±1% and from 1±1 to 20±18%, respectively. In contrast, the relative error of state 4 respiratory rate, ADP/O ratio and RCR obtained with denoised data was not significantly different from zero regardless the sampling rate.

In IFM the results obtained for the relative errors using either raw or denoised data were similar to those reported for SSM for each condition investigated.

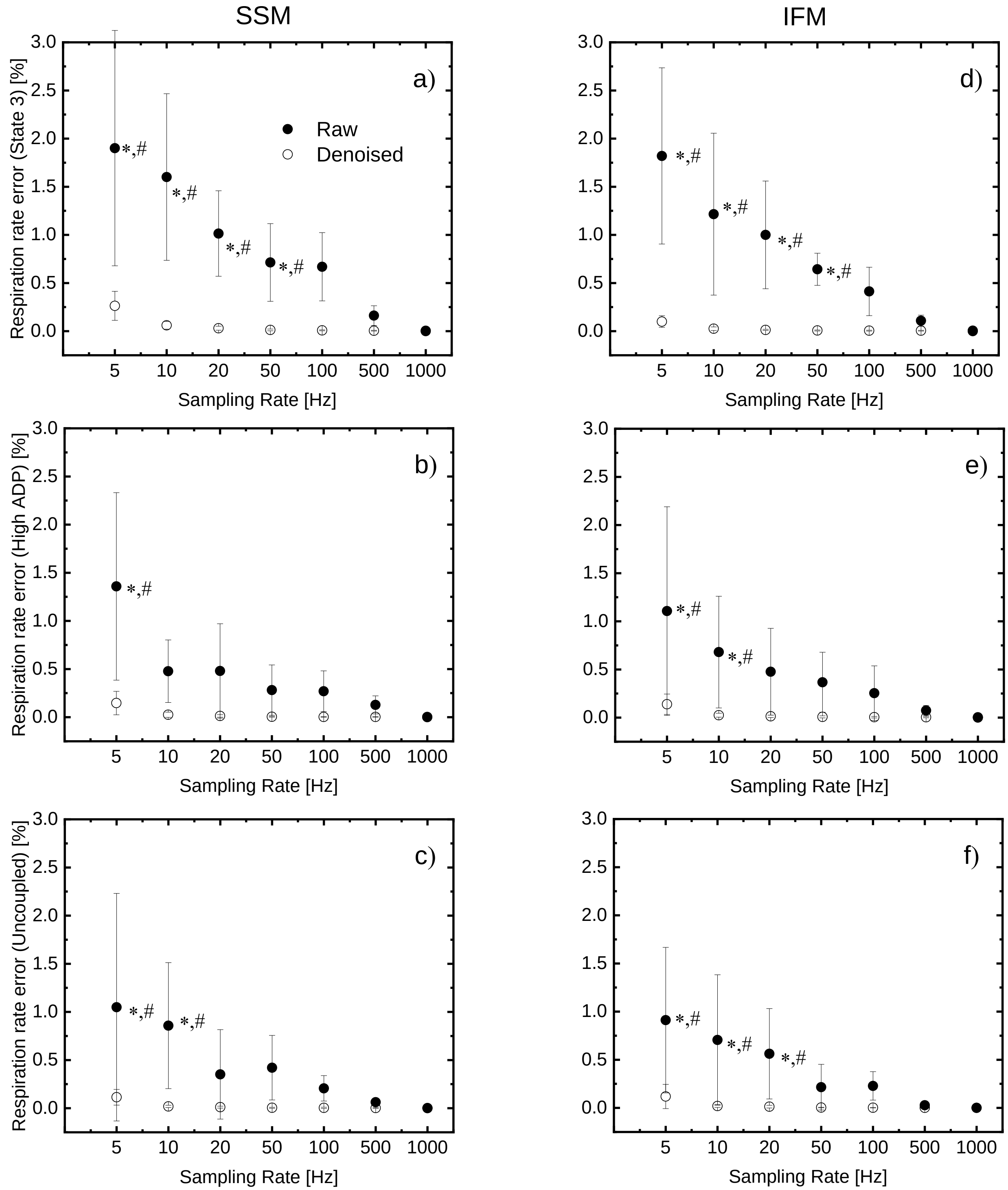

Figure 4. Effect of the sampling rate on the percentage error in calculating bioenergetic outputs: state 3 respiratory rate with an unsaturated (a) and saturated concentration of ADP (b) as well as uncoupled respiration rate (c) using raw and denoised data of SSM; state 3 respiratory rate with an unsaturated (d) and saturated concentration of ADP (e) as well as uncoupled respiration rate (f) using raw and denoised data of IFM. Data are reported as mean ± SD (n=10).
Influence of sampling rate ($p<10^{-3}$) (*) Statistically different from relative error obtained with raw data at 1000 Hz.
Influence of denoise process at different sampling rate ($p<10^{-3}$) (#) Statistically different from denoised data at the same sampling rate.

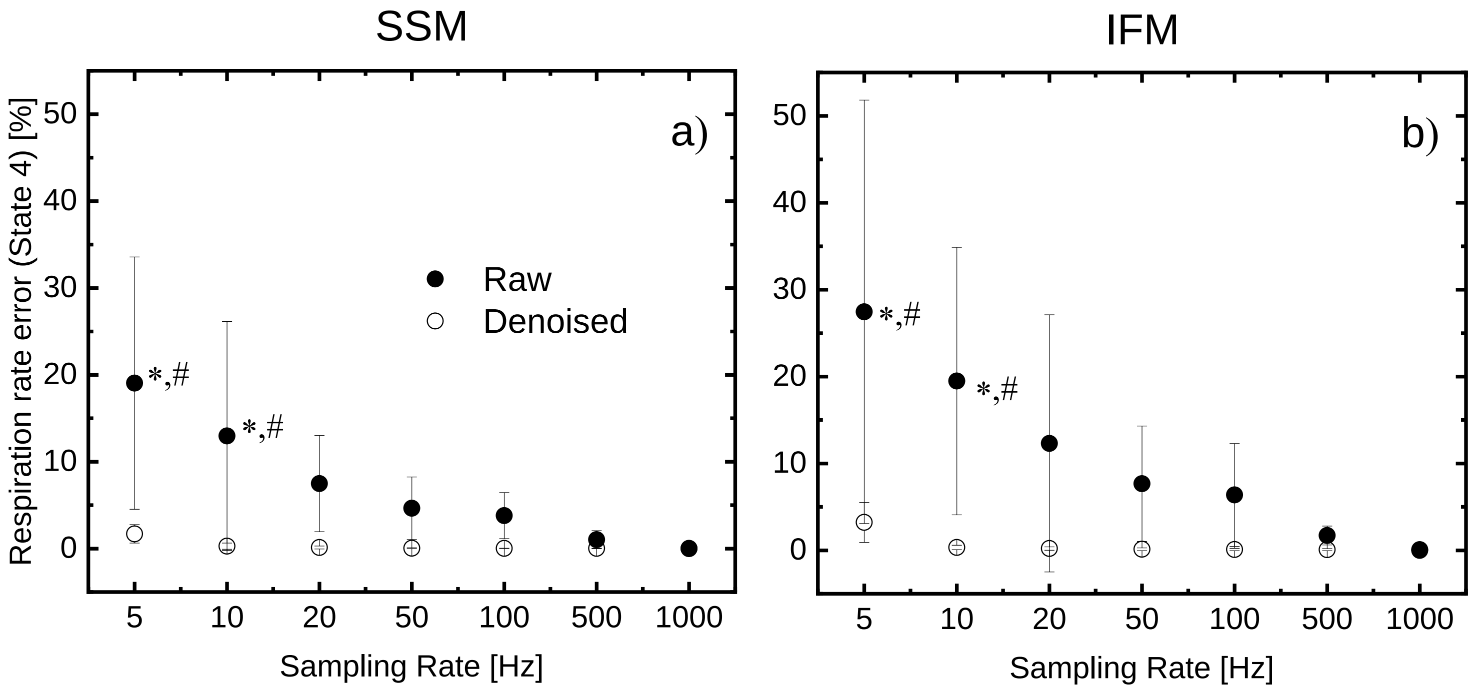

Figure 5. Effect of the sampling rate on the percentage error in calculating state 4 respiratory rate using raw and denoised data of SSM (a) and IFM (b). Data are reported as mean ± SD (n=10).

Influence of sampling rate ($p<10^{-3}$) (*) Statistically different from relative error obtained with raw data at 1000 Hz.

Influence of denoise process at different sampling rate ($p<10^{-3}$) (#) Statistically different from denoised data at the same sampling rate.

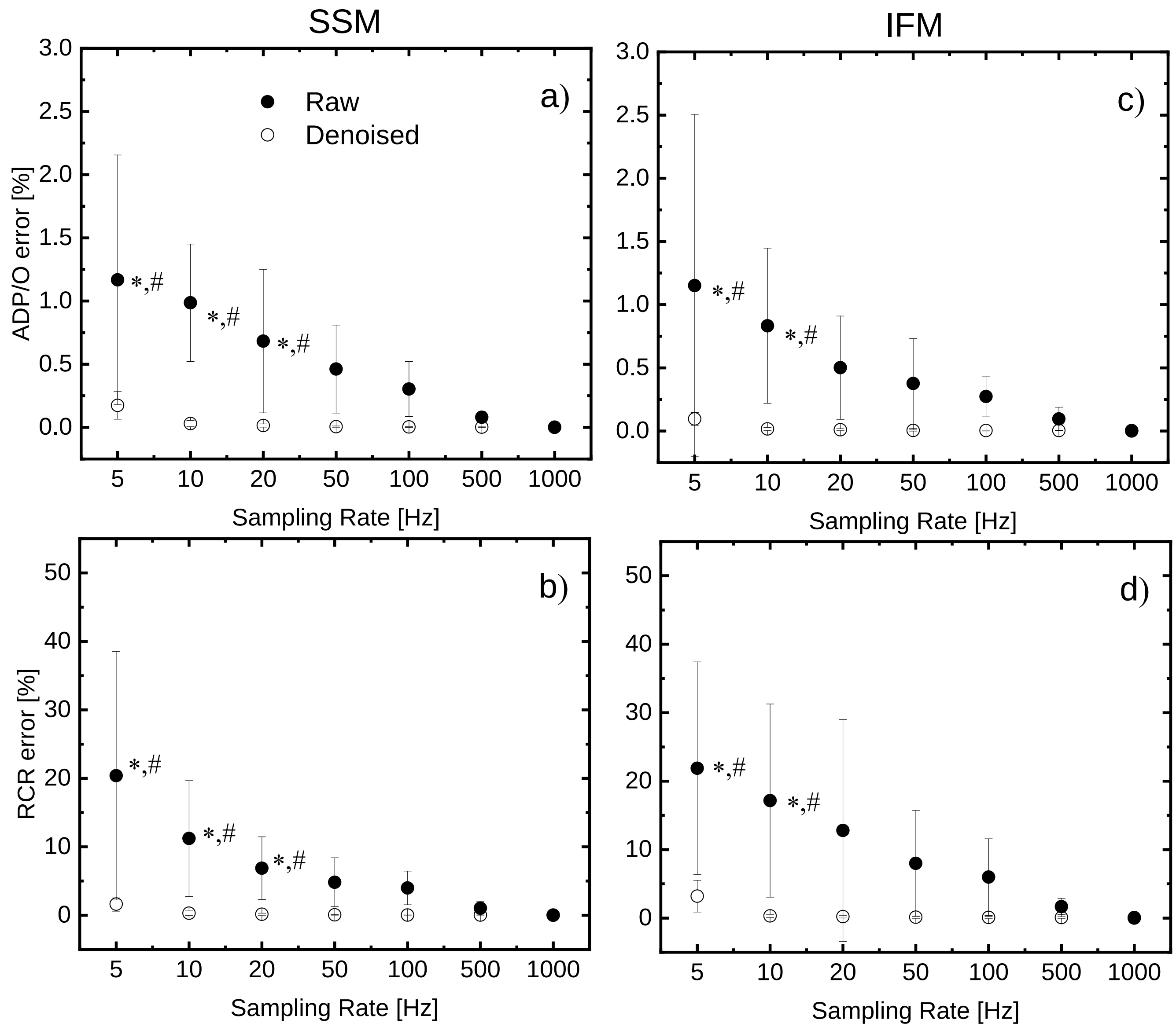

Figure 6. Effect of the sampling rate on the percentage error in calculating bioenergetic outputs: ADP/O ratio (a) and RCR (b) using raw and denoised data of SSM; ADP/O ratio (c) and RCR (d) using raw and denoised data of IFM. Data are reported as mean ± SD (n=10). Influence of sampling rate ($p<10^{-3}$) (*) Statistically different from relative error obtained with raw data at 1000 Hz. Influence of denoise process at different sampling rate ($p<10^{-3}$) (#) Statistically different from denoised data at the same sampling rate.

4. Discussion

A graphical user interface was developed and integrated with an analog-to-digital converter to perform data acquisition, visualization, and processing of a polarographic system. GUI can be used to calculate respiration rates, RCR, and ADP/O ratios from oxygen kinetics measured with the polarographic system. A filter was applied to the polarographic data for real time visualization. The GUI includes signal processing to denoise the data to have a relative error in calculating the respiration rates, RCR, and ADP/O ratio lower than 0.5% with low sampling rates (10 Hz) in comparison to the results obtained with raw data at 1000 Hz. The integrated tools of the GUI were used to overcome the limitations related to the analysis of data of polarographic systems without a digitized and software components.

In this study, oxidative phosphorylation characteristics of both populations of skeletal muscle mitochondria were similar to those previously determined by our group using the same polarographic system, animal model, and experimental protocol [24, 36]. Other systems are based on the same oxygraph [14-19, 21, 22, 26], Clark electrode [14, 17, 26, 34, 42], and similar volume of the metabolic chamber [26, 42, 44] of our study.

4.1.Graphical user interface

Several polarographic systems without a digitized component or software to process the data are used by the research community [14, 27-33, 36] and the analysis of the data is more time consuming than the commercial integrated system. In our work, the integrative approach proposed allows a fast and accurate calculation of the respiration rates and ADP/O ratios. These calculations can not only be performed on data collected by our GUI but also from data recorded by other digitized systems.

The GUI of our study can be also used for other analog polarographic systems with a compatible data acquisition device which require only minor changes in the parameter settings of the GUI. Furthermore, the data acquisition device (NI-DAQ, USB-6001) used in this study allow to use any analog polarographic system with an output voltage within the ±10V range. The file format to store and analyze the data is comma separated values, which is a common data exchange format.

4.2.Effect of Sampling rate

The Gaussian distribution of the difference between the raw and denoised data (Fig. 3b) indicates that the noise is independent of the time and the denoising procedure used in our work is acceptable. The efficiency of the denoising process in minimizing the noise and sampling rate of the recorded data is related to the YSI 5300 model. Noise could be related to the data acquisition hardware, magnetic stirrer, and other laboratory equipment in the vicinity. The approach proposed for our system to evaluate the noise and identify the optimal sampling rate can be generalized whereas other polarographic systems may require a different signal filtering.

To minimize the relative error in calculating the respiration rates, ADP/O ratios and RCR obtained with raw data collected at low sampling rate (Fig. 4 and 5), a signal processing was applied to the data. Thus, the relative error in calculating the respiration rates, RCR, and ADP/O ratio values obtained at 1000 Hz (Table 1) was negligible even for low sampling rate.

The state 4 respiration rate relative error is the most sensitive in comparison to the other respiration rates errors to the sampling rate changes (Fig. 5) because the absolute error is similar for all respiration rates and state 4 respiration rate is approximately 17-30 fold lower than the other respiration rates used to normalize the absolute error (Table 1).

In addition, the calculation of the state 4 respiration rate (Fig. 5) affects the calculation of ADP/O ratio and RCR (Fig. 6). For these ratios, the relative error increases with a decrease of the sampling rate, because of the increase error in determining state 4 respiration rate. This rate did not only directly affect RCR (State 3/State 4), but also ADP/O ratio because it was used to determine the intersection point required to quantify the oxygen utilized to phosphorylate the ADP injected. Thus, state 4 respiratory rate error can be used to identify the best sampling rate assuring a low relative error for all biochemical data extracted from the oxygen kinetics. The use of denoised data allowed to have a state 4 respiratory rate relative error lower than 3±2% at a sampling rate of 5Hz. This error value was the highest among all errors obtained with the respiration rates, ADP/O ratios, and RCR and it was not significantly different from zero (Fig. 5). Thus, this sampling rate represents a good compromise between data accuracy and resolution. Reducing the sampling rate by 100 fold is convenient when these kinetics data are used for computational methods to study the regulation of oxidative phosphorylation under physiological and pathophysiological conditions [45-48]. In particular, the estimate of the parameters of computational models of mitochondrial energy metabolism requires oxygen kinetics data which in case of a sampling rate of 1000 Hz for an experiment of 5 minutes implies the utilization of large amount of data (i.e. $3\ 10^5$). Thus, a reduced sampling rate that does not significantly affect the nature of the kinetics is desirable to efficiently use these computational methods.

4.3.Conclusion

The integrated approach proposed was used to digitize, visualize, and analyze data by a graphical user interface designed for analog polarographic systems. Software with the GUI is available to analyze the data recorded with other polarographic systems. The graphical user interface overcomes cumbersome calculations to extract bioenergetic data from oxygen kinetics, enhance the accuracy of RCR and ADP/O ratio, and optimize the decimation of kinetic data for computational applications.

Conflict of Interest

The authors declare that they have no conflict of interest associated with this manuscript.

Acknowledgments

We are grateful to Garett Johnson and George Micros of the Old Dominion University for their assistance in digitizing the system. This research was supported by National Institute of Arthritis and Musculoskeletal and Skin Diseases (NIH-NIAMS) and National Institute of Diabetes and Digestive and Kidney (NIH-NIDDK) under award number K25AR057206 and P30DK027651, respectively; and the Center for Mitochondrial Disease, Case Western Reserve University.

Supplemental material

Supplementary material includes the file examples and file to install the graphical user interface. The material is accessible in the data repository "Mendeley Data" with doi:10.17632/zb3d696s5c.1.

References

1. B., Chance, G.R., Williams, W.F., Holmes, J., Higgins, Respiratory enzymes in oxidative phosphorylation, J. of Biol. Chem. 217(1) (1955) 439-51.
2. L.C., Clark Jr, R., Wolf, D., Granger, Z., Taylor, Continuous recording of blood oxygen tensions by polarography, J of Appl. Physiol. 6 (1953) 189-193.
3. L.C., Clark Jr., Monitor and control of blood and tissue oxygen tensions, Transactions of the american society of artificial internal organs, 2(41) (1956).
4. I., Fatt, Theory of operation and its application in biology, medicine, and technology, In: Polarographic Oxygen Sensors. USA: Robert E. Kreiger Publications (1982).
5. E., Gnaiger, H., Forstner (eds), Aquatic and physiological applications, In: Polarographic Oxygen Sensors. New York: Springer-Verlag. (1983) 1-370.
6. L.J.C., Wong, Mitochondrial Disorders: Biochemical and molecular analysis, Human press (2012).
7. Walker D, Polarographic measurement of oxygen, In: Photosynthesis and production in a changing environment. Dordrecht: Springer (1993).
8. J., Whelan, M.W., Murcha, Plant mitochondria methods and protocols. methods in molecular biology, Human press (2015).
9. A., Barrientos, F., Fontanesi, F., Díaz, Evaluation of the mitochondrial respiratory chain and oxidative phosphorylation system using polarography and spectrophotometric enzyme assays, Curr Protoc Hum Genet Chapter 19:Unit19.3 (2009).
10. E., Gnaiger, Polarographic oxygen sensors, the oxygraph and high-resolution respirometry to assess mitochondrial function, In: Mitochondrial Dysfunction in Drug-Induced Toxicity (J.A., Dykens, Y., Will eds) John Wiley & Sons, Inc, Hoboken, NJ. (2008) 327-52.

11. J.F., O'Toole, H.V., Patel, C.J., Naples, H., Fujioka, C.L., Hoppel, Decreased cytochrome c mediates an age-related decline of oxidative phosphorylation in rat kidney mitochondria, Biochem. J. 427(1) (2010) 105-12.
12. M., Pelletier, L.K., Billingham, M., Ramaswamy, R.M., Siegel, Extracellular flux analysis to monitor glycolytic rates and mitochondrial oxygen consumption, In: Methods in Enzymology, Ch 7 542 (2014) 125-149.
13. D., Walker, The use of the oxygen electrode and fluorescence probes in simple measurements of photosynthesis, Research Institute for Photosynthesis, University of Sheffield; 2nd Ed. (1987) 1-145.
14. K., Anflous-Pharayra, N., Lee, D.L., Armstrong, W.J., Craigen, VDAC3 has differing mitochondrial functions in two types of striated muscles, Biochim. et Biophys. Acta. 1807(1) (2011) 150-156.
15. W.A., Baseler, E.R., Dabkowski, R., Jagannathan, D., Thapa, C.E., Nichols, D.L., Shepherd, T.L., Croston, M., Powell, T.T., Razunguzwa, S.E., Lewis, D.M., Schnell, J.M., Hollander, Reversal of mitochondrial proteomic loss in Type 1 diabetic heart with overexpression of phospholipid hydroperoxide glutathione peroxidase, Am. J. Physiol. Regul. Integr. Comp. Physiol. 304(7) (2013) R553-R565.
16. E.R., Dabkowski, C.L., Williamson, V.C., Bukowski, R.S., Chapman, S.S., Leonard, C.J. Peer, P.S., Callery, J.M., Hollander, Diabetic cardiomyopathy-associated dysfunction in spatially distinct mitochondrial subpopulations, Am J Physiol Heart Circ Physiol 296 (2009) H359-H369.
17. O., Hashizume, S., Ohnishi, T., Mito, A., Shimizu, K., Ishikawa, K., Nakada, M., Soda, H. Mano, S., Togayachi, H., Miyoshi, K., Okita, J., Hayashi, Epigenetic regulation of the

nuclear-coded GCAT and SHMT2 genes confers human age-associated mitochondrial respiration defects, Sci Rep 5 (2015) 10434.

18. N., Kaneko, T., Rikimaru, T., Fujimura, S., Mori, S., Hidaka, H., Kaya, Preparation of rat gingival mitochondria with an improved isolation method, Intl. J. of Dentistry. 11, (2010) 275103.
19. X., Pan, J., Liu, T., Nguyen, C., Liu, J., Sun, Y., Teng, M.M., Fergusson, I.I., Rovira, M., Allen, D.A., Springer, A.M., Aponte, M., Gucek, R.S., Balaban, E., Murphy, T., Finkel, The physiological role of mitochondrial calcium revealed by mice lacking the mitochondrial calcium uniporter, Nature Cell Biology 15(12) (2013) 1464-1472.
20. P., Singh-Rawal, O., Zsiros, S., Bharti, G., Garab, A., Jajoo, Mechanism of action of anions on the electron transport chain in thylakoid membranes of higher plants, J. Bioenerg. Biomembr. 43(2) (2011) 195-202.
21. L., Vergani, A., Malena, P., Sabatelli, E., Loro, L., Cavallini, P., Magalhaes, L., Valente, F., Bragantini, F., Carrara, B., Leger, J., Poulton, A.P., Russell, I.J., Holt, Cultured muscle cells display defects of mitochondrial myopathy ameliorated by anti-oxidants, Brain 130(10) (2007) 2715-2724.
22. H.Y., Zhu, S.W., Wang, L., Liu, Y.H., Li, R., Chen, L., Wang, J., Holliman, A mitochondrial mutation A4401G is involved in the pathogenesis of left ventricular hypertrophy in Chinese hypertensives, Euro J. of Human Genetics. 17(2) (2009) 172-178.
23. A., Panov, Z., Orynbayeva, Determination of mitochondrial metabolic phenotype through investigation of the intrinsic inhibition of succinate dehydrogenase, Anal. Biochem. 552 (2018) 30-37.

24. N., Lai, C., Kummitha, C.L., Hoppel, Defects in skeletal muscle subsarcolemmal mitochondria in a non-obese model of type 2 diabetes mellitus, PLoS One 12(8) (2017) e0183978.

25. S., Munusamy, J.M., do Carmo, J.P., Hosler, J.E., Hall. Obesity-induced changes in kidney mitochondria and endoplasmic reticulum in the presence or absence of leptin, Am. J. Physiol. Renal. Physiol. 309 (2015) F731-F743.

26. M.G., Rosca, E.J., Vazquez, J., Kerner, W., Parland, M.P., Chandler, W., Stanley, H.N., Sabbah, C.L., Hoppel, Cardiac mitochondria in heart failure: decrease in respirasomes and oxidative phosphorylation, Cardiovasc. Res. 80(1) (2008) 30-9.

27. A.M., Silva, P.J., Oliveria, Evaluation of respiration with Clark type electrode in isolated mitochondria and permeabilized animal cells, In: Mitochondrial Bioenergetics: Methods and Protocols, edited by Palmeria CM Moreno AJ. Springer Science, (2012) 7-20.

28. H.A., Funes, N., Apostolove, F., Alegre, A., Blas-Garcia, A., Alvarez, M., Marti-Cabrera, J.V., Esplugues, Neuronal bioenergetics and acute mitochondrial dysfunction, Journal of Infectious Diseases 210(9) (2014) 1385-95.

29. A., Kopustinskas, R., Adaskevicius, A., Krusinskas, D.M., Kopustinskiene, J., Liobikas, A., Toleikis, A User-friendly PC-based data acquisition and analysis system for respirometric investigations, Comput. Methods Programs Biomed. 82(3) (2006) 231-237.

30. Y., Liu, D.S., Barber, P., Zhang, B., Liu, Complex II of the mitochondrial respiratory chain is the key mediator of divalent manganese-induced hydrogen peroxide production in microglia, Toxicological Sciences 132(2) (2013) 298-306.

31. K., Mamchaoui, G., Saumon, A method for measuring the oxygen consumption of intact cell monolayers, Am. J. Physiol. Lung Cell Mol. Physiol. 278(4) (2000) L858-L863.

32. C., Diepart, J., Verrax, P.B., Calderon, O., Feron, B.F., Jordan, B., Gallez, Comparison of methods for measuring oxygen consumption in tumor cells in vitro, Anal. Biochem. 396(2) (2010) 250-6.
33. S., Ödman, N., Lund, Data acquisition and information processing in MDO oxygen electrode measurement of tissue oxygen pressure, Acta Anaesthesiol. Scand. 24(3) (1980) 161-165.
34. M.V., Orna, Chapter 15: Oxygen Electrode, In: Electrochemistry, Past and Present. Edited by: Stock JT Orna MV. Washington, D.C.: American Chemical Society (1989) 196-210.
35. National Research Council. Guide for the care and use of laboratory animals, 8th Ed. Washington, DC: National Academies Press (2011).
36. N., Lai, M.C., Kummitha, M.G., Rosca, H., Fujioka, B., Tandler, C.L., Hoppel, Isolation of mitochondrial subpopulations from skeletal muscle: Optimizing recovery and preserving integrity, Acta Physiol. (Oxf) (2018) e13182.
37. O.H., Lowry, N.J., Rosebroug, A.L., Farr, R.J., Randall, Protein measurement with the Folin phenol reagent, J. Biol. Chem. 193 (1) (1951) 265-275.
38. J.B., Chappell, The oxidation of citrate, isocitrate and cis-aconitate by isolated mitochondria, Biochem. J. 90(2) (1964) 225-237.
39. MATLAB 2016a. Natick, Massachusetts: The MathWorks Inc. (2010).
40. C.L., Hoppel, J., DiMarco, B., Tandler, Riboflavin and rat hepatic cell structure and function. Mitochondrial oxidative metabolism in deficiency states. J. Biol. Chem. 254 (1979) 4164-4170.
41. W. M., Haynes, D. R., Lide, T. J., Bruno, CRC Handbook of Chemistry and Physics, 97th Edition (2017).

42. R.J., Tomec, C.L., Hoppel, Carnitine palmitoyltransferase in bovine fetal heart mitochondria, Arch. Biochem. Biophys. 170(2) (1975) 716-23.

43. R.W., Estabrook, Mitochondrial respiratory control and polarographic measurement of ADP/O ratios, Methods Enzymol. 10 (1967) 41-47.

44. R.E., Justice, T., Utsunomiya, M.M., Krausz, C.R., Valer, D., Shepro, H.B., Hechtman, A miniaturized chamber for the measure of oxygen consumption. J. Appl. Physiol.: Respirat. Environ. Exercise Physiol. 52(2) (1982) 488-490.

45. J.N., Bazil, V.R., Pannala, R.K., Dash, D.A., Beard, Determining the origins of superoxide and hydrogen peroxide in the mammalian NADH:ubiquinone oxidoreductase, Free Radic. Biol. Med. 77 (2014) 121-9.

46. B., Korzeniewski, Regulation of oxidative phosphorylation during work transitions results from its kinetic properties. J. Appl. Physiol. 116(1) (2014) 83-94.

47. Y., Li, N., Lai, J.P., Kirwan, G.M., Saidel, Computational model of cellular metabolic dynamics in skeletal muscle fibers during moderate intensity exercise, Cell. Mol. Bioeng. 5(1) (2012) 92-112.

48. X., Zhang, R.K., Dash, E.R., Jacobs, A.K.S., Camara, A.V., Clough, S.H., Audi, Integrated computational model of the bioenergetics of isolated lung mitochondria, PLoS One 13(6) (2018) e0197921.